Supporting Information

Capacitive Conjugated Ladder Polymers for Fast-Charge and -Discharge Sodium-ion Batteries and Hybrid Supercapacitors

Yuan Chen, Hongyang Li, Mi Tang, Shuming Zhuo, Yanchao Wu, Erjing Wang, Shimin Wang*, Chengliang Wang* and Wenping Hu**

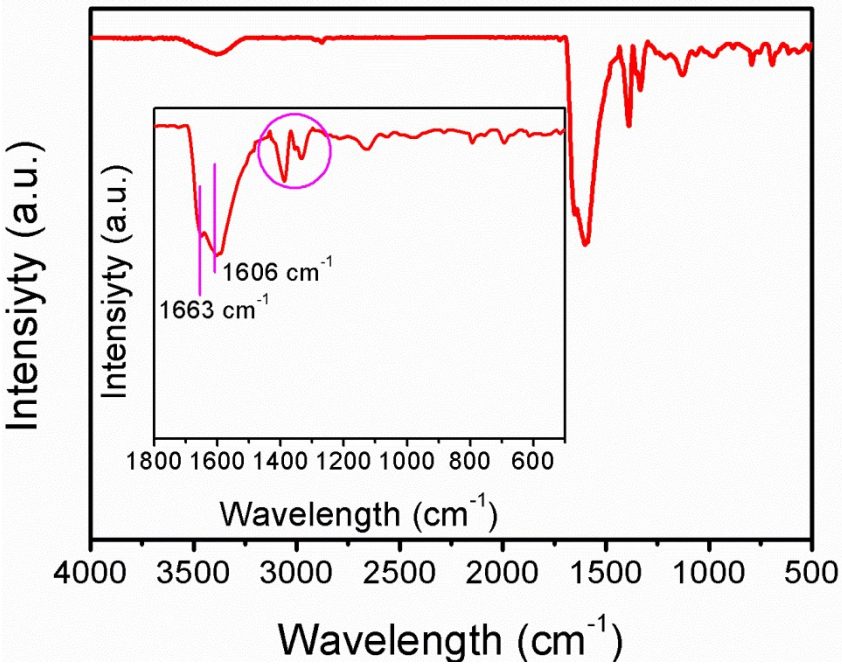

Fig. S1 FT-IR spectra of PYT-TABQ with the inset showing the region of low wavelength. The peaks at 1663 and 1606 cm^{-1} are assigned to C=O and C=N groups, respectively. The peaks at around 1330-1430 cm^{-1} (the elliptic region) can be attributed to the C-N bonds.

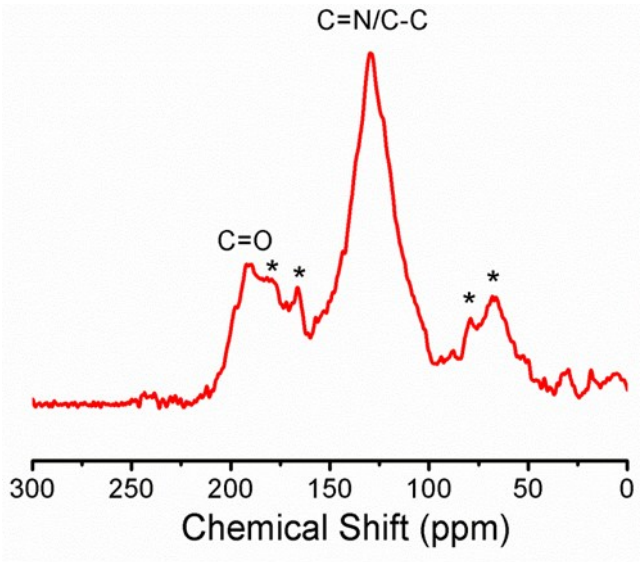

Fig. S2 Solid-state ^{13}C-NMR spectrum of PYT-TABQ and the signal assignments (*side peaks). In ^{13}C-NMR spectrum, the peak at 192 ppm originates from the C=O groups and the signal at around 120~145 ppm is assigned to the superposition of C=C/C-C and C=N/C-N groups.

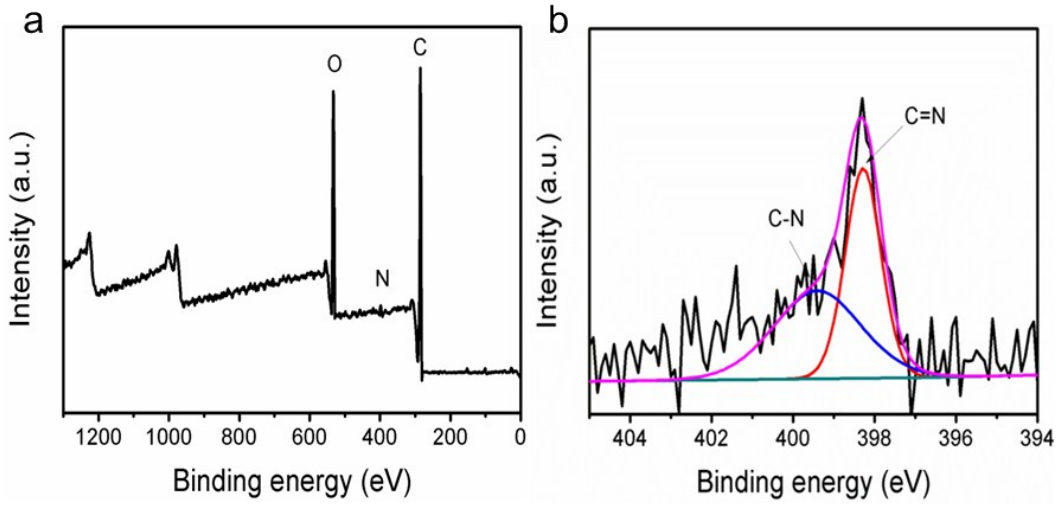

Fig. S3 a) XPS spectrum of PYT-TABQ, showing the existence of C, N and O. b) XPS spectra of N 1s spectrum of PYT-TABQ, indicating the coexistence of C=N and C-N bonds.

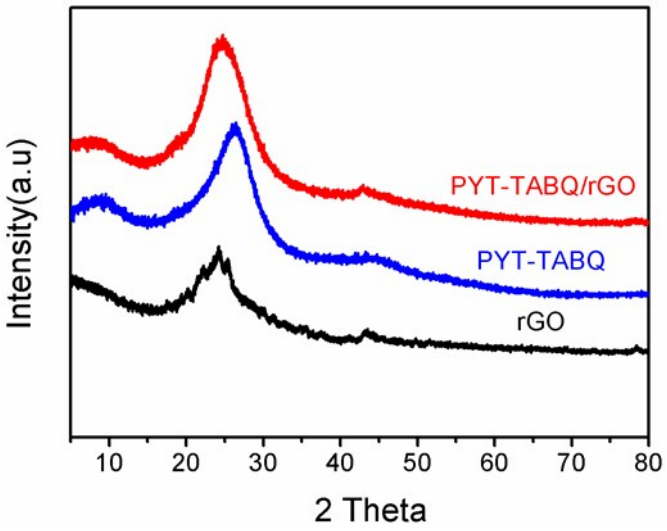

Fig. S4 XRD patterns of the PYT-TABQ/rGO, PYT-TABQ and rGO.

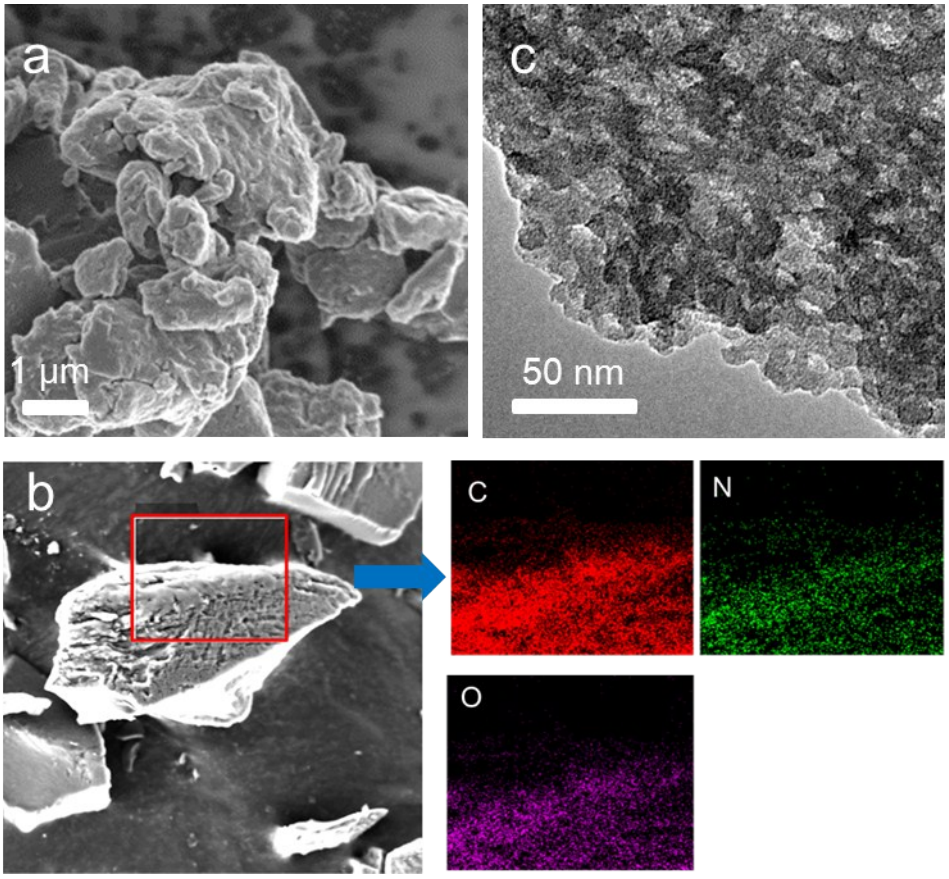

Fig. S5 a) SEM image of PYT-TABQ powders and b) corresponding elemental C, N and O mapping. c) TEM image of PYT-TABQ.

Table S1. Elemental analysis results of PYT-TABQ. The calculated results are obtained by using polymerization degree of 6, the ending groups are dominantly -NH_2. The C/N ratio of PYT-TABQ is consistent with the calculated value.

Sample		N %	C %	H %	O%	C/N
PYT-TABQ	Calculated results	17.15	71.1	1.95	9.8	4.15
	Found	16.54	68.40	3.59	11.4	4.14

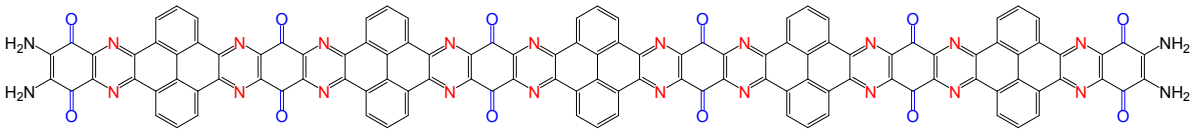

n=6 calculated: C:71.1; H:1.95; N:17.15; O:9.8 C/N=4.15

Fig. S6 The average chemical formula of PYT-TABQ. Based on the results of EA and FT-IR, both ends of the PYT-TABQ chain probably ended with amino groups. The PYT-TABQ has a molecular weight of 358 g mol^{-1} per repeating unit. Therefore, the theoretical specific capacity can be calculated to be: $C=26801\times n/M_w=299.3$ (mAh g^{-1}, n and M_w are the number of electrons and molecular weight, respectively), in view of the four electrons transferred.

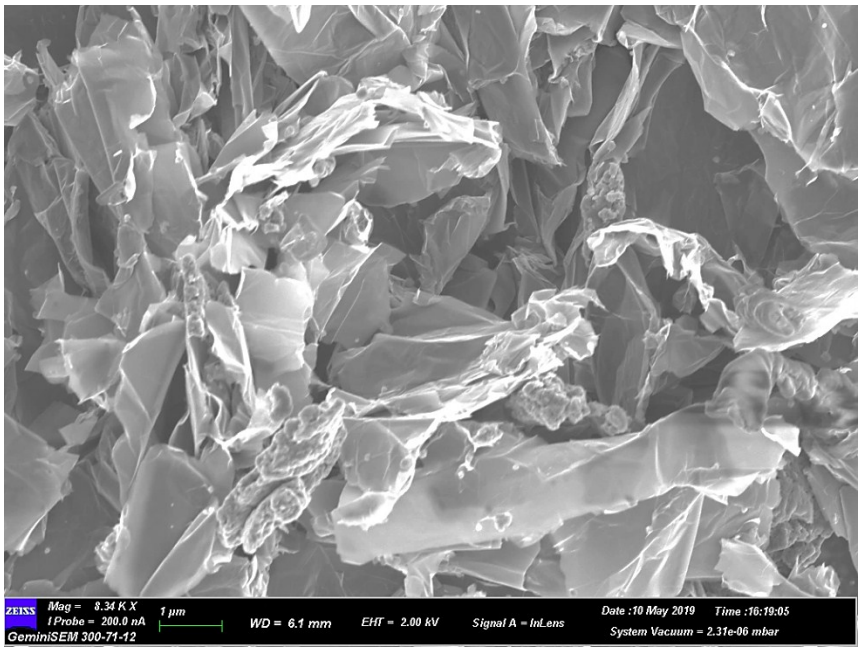

Fig. S7 SEM images of PYT-TABQ/rGO.

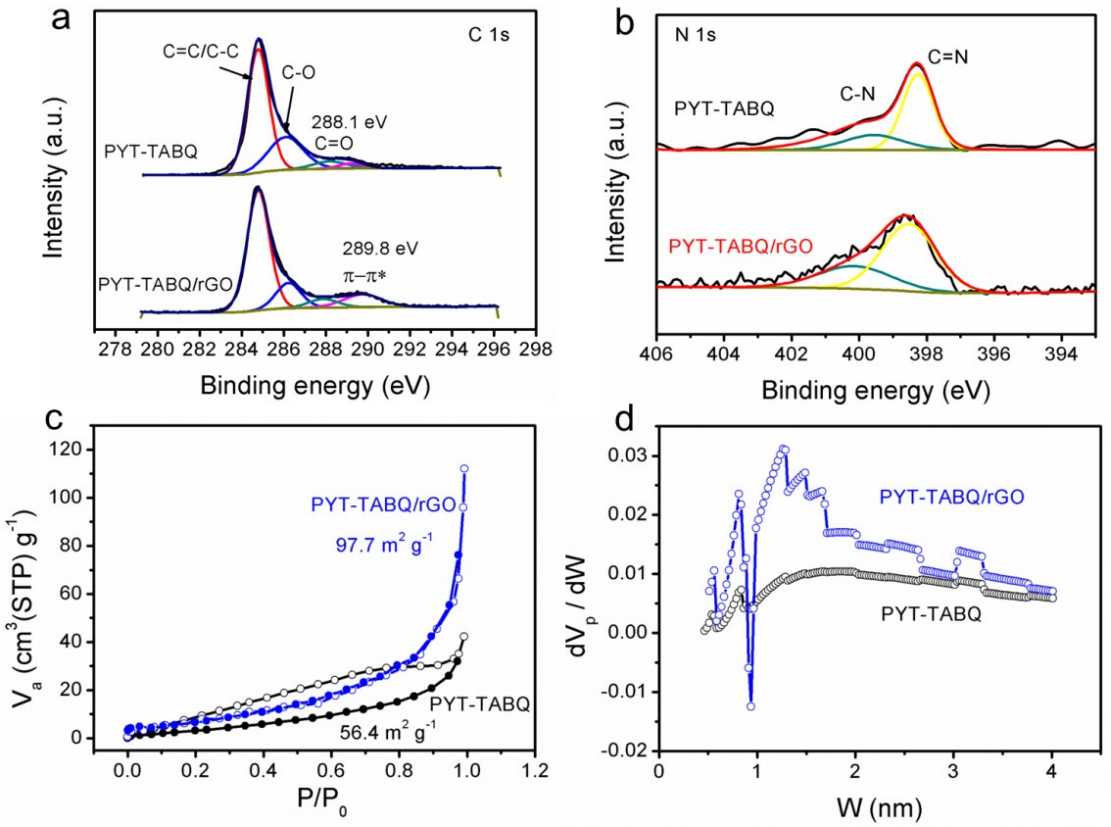

Fig. S8 XPS C1s (a) and N1s (b) spectrum of PYT-TABQ and PYT-TAB/rGO; the nitrogen adsorption isotherms at 77K (c) and corresponding pore diameter distribution (d) of PYT-TABQ and PYT-TABQ/rGO.

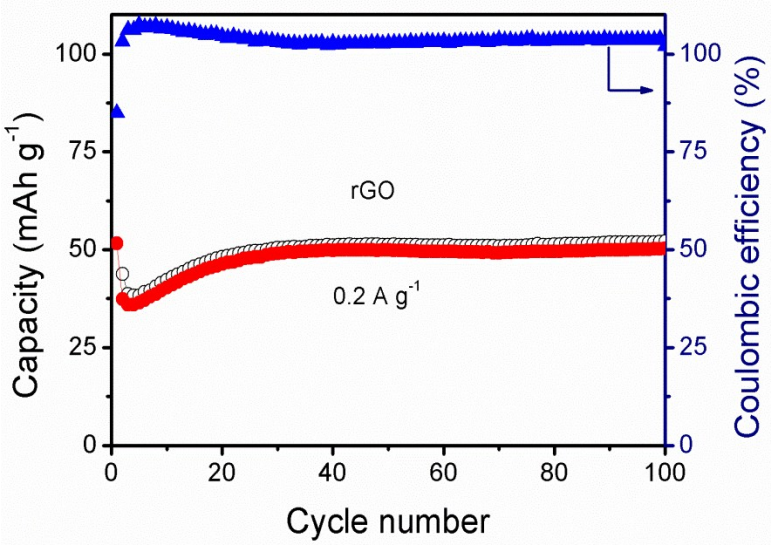

Fig. S9 The electrochemical performance of rGO (1.0~3.5 V), delivering a capacity of about 50 mAh g^{-1}. The rGO electrode was prepared by mixing rGO with PVDF in a weight ratio of 3:1. Hence, the capacity contribution from rGO in the composite electrodes should be lower than 25 mAh g^{-1}.

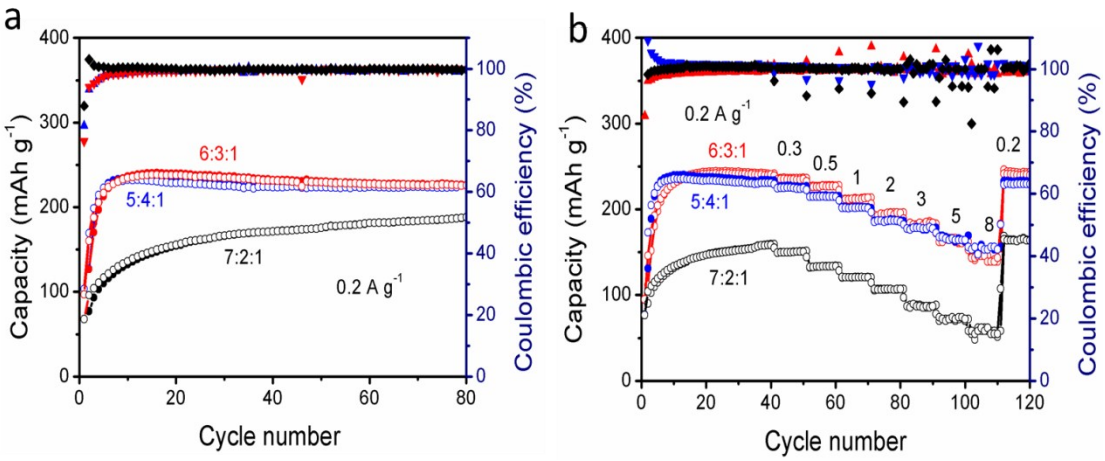

Fig. S10 Cycling and rate performances of PYT-TABQ/rGO composites with different contents of rGO. When the content of PYT-TABQ increased to 70% (the content of rGO decreased to 20% accordingly), the capacity and rate capability of the composites decreased significantly. In view of the low capacity contribution of rGO, the decrease of the composite electrode should be ascribed to the relative lower electric conductivity of the polymer. On the other hand, further increase of the content of rGO did not give higher capacity and rate performance. The electrode materials with 30% of the amount of rGO was hence used for further study.

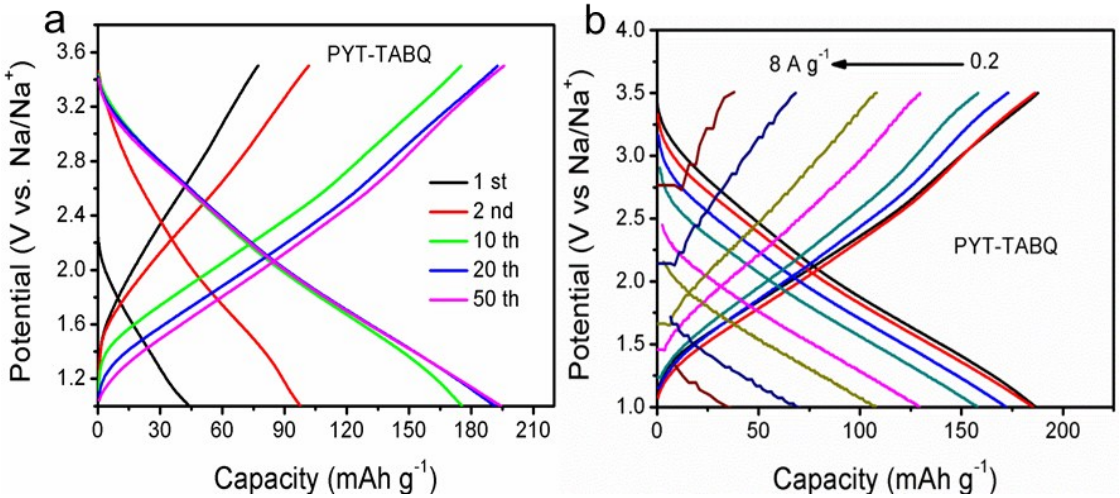

Fig. S11 a) The discharge-charge curves of PYT-TABQ at 0.2 A g^{-1} and b) at different current densities. The potential window is 1.0-3.5 V.

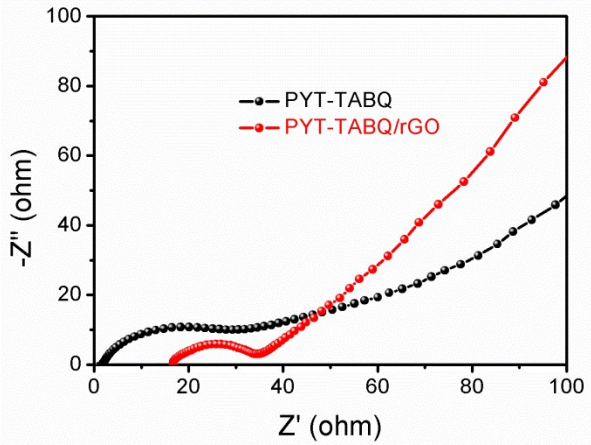

Fig. S12 The Nyquist plots of the PYT-TABQ and PYT-TABQ/rGO after the first discharging. The resistance values were obtained from the diameters of semi-circles in the high-frequency range. Obviously, a smaller resistance indicates a faster electron transfer rate. The results suggested the lower resistance of PYT-TABQ/rGO than that of PYT-TABQ.

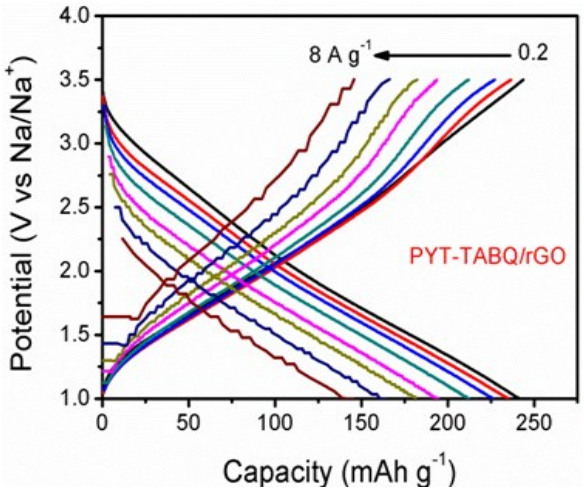

Fig. S13 The discharge-charge curves of PYT-TABQ/rGO at different current densities.

Table S2. Comparison of the Na-storage performance of PYT-TABQ/rGO with representative organic cathodes in literatures.

Materials	Performance at low rate		Performance at high rate		Retention (current, cycles)	Ref.
	Current density ($A\ g^{-1}$)	Capacity ($mAh\ g^{-1}$)	Current density ($A\ g^{-1}$)	Capacity ($mAh\ g^{-1}$)		
BPOE	0.01	~200	1	~90	80 % (1 $A\ g^{-1}$, 7000)	[1]
PAQS	1 C	~220	16 C	~180	100 % (8 C, 200)	[2]
PANS	0.1	~120	0.8	~76	~	[3]
PPy-S	0.04	85	~	~	88 % (0.1 $A\ g^{-1}$, 100)	[4]
DAPT-TFP-CPF	0.1	~150	1	~120	100 % (1 $A\ g^{-1}$, 1300)	[5]
PBQS	0.05	~260	~	~	68 % (0.05 $A\ g^{-1}$, 100)	[6]
P(AN-NA)	0.05	~180	~	~	96 % (0.05 $A\ g^{-1}$, 50)	[7]
PMDI-DHAP	0.1 C	~73	~	~	50 % (0.05 C, 50)	[8]
PI	0.05	126	0.8	106	58 % (0.8 $A\ g^{-1}$, 50)	[9]
PAQI	0.05	197	1	130	94 % (0.05 $A\ g^{-1}$, 50)	[10]
PAQS/rGO	0.112 (0.5 C)	~150	1.125 (5C)	74	71.4 % (225 $mA\ g^{-1}$, 100)	[11]
PI/rGO	0.04	240	1	116	73 % (1 $A\ g^{-1}$, 1000)	[12]
PYT-TABQ/rGO	0.2	245	1	~210	98 % (1 $A\ g^{-1}$, 1400)	**This work**

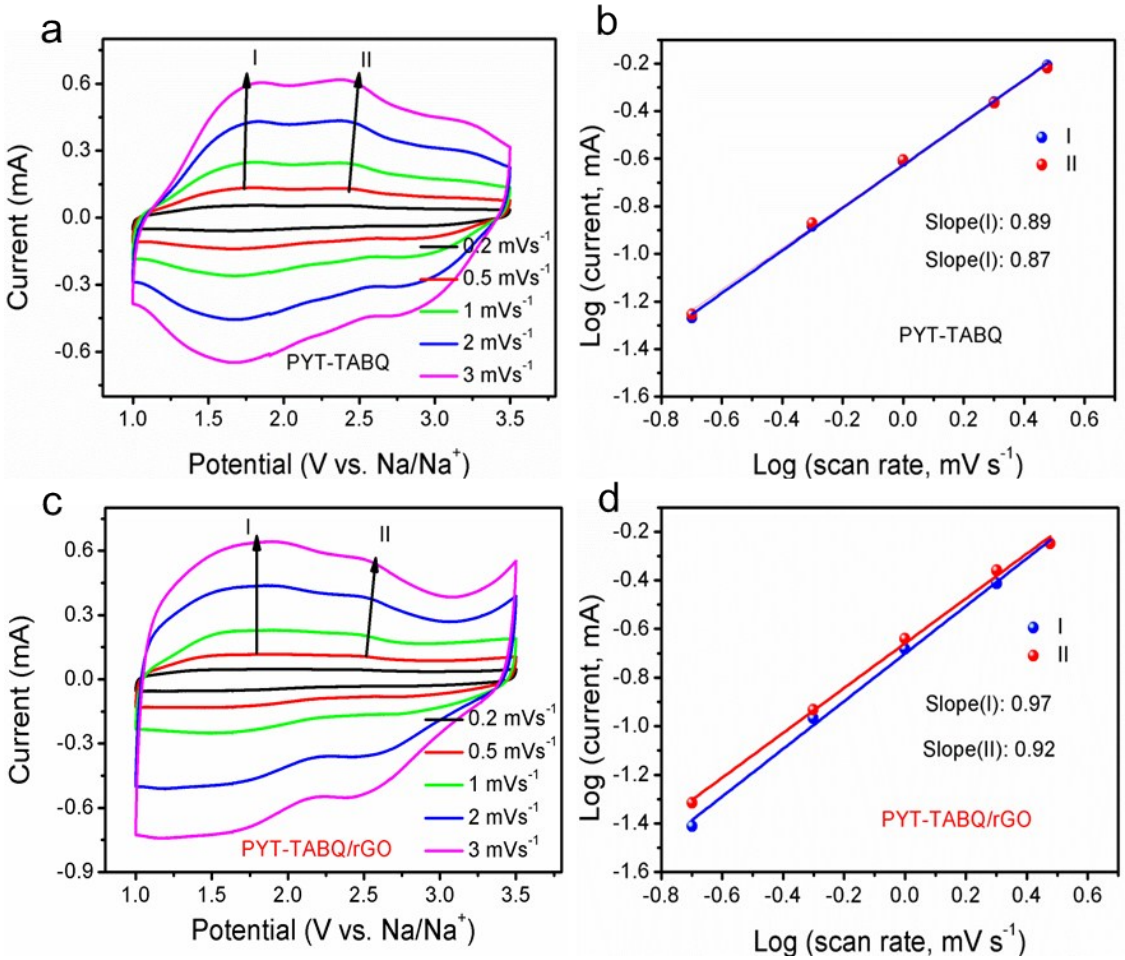

Fig. S14 a, c) CV curves at different scan rates from 0.2 to 3 mV/s for a) PYT-TABQ and c) PYT-TABQ/rGO. b, d) b value at different scan rates, calculated from peak current and scan rate from a) and c).

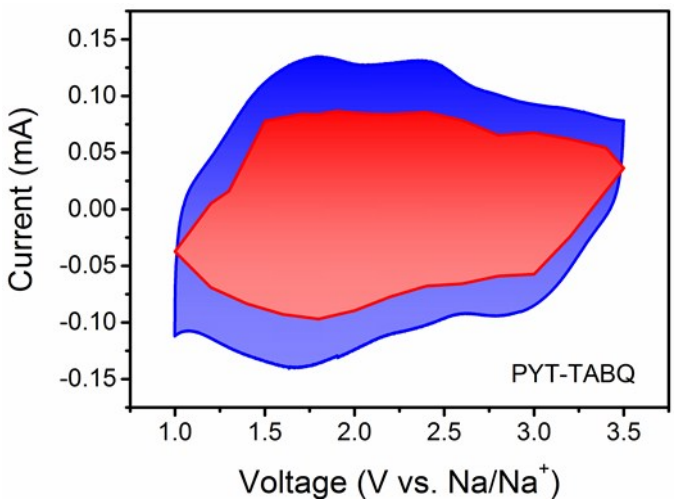

Fig. S15 The contribution of capacitive (red area) and diffusion controlled current to the total current (blue area) at 0.5 mV s^{-1}. The quantitative contribution of capacitive processes for the PYT-TABQ electrode was about 55.9 % at a scan rate of 0.5 mV s^{-1}.

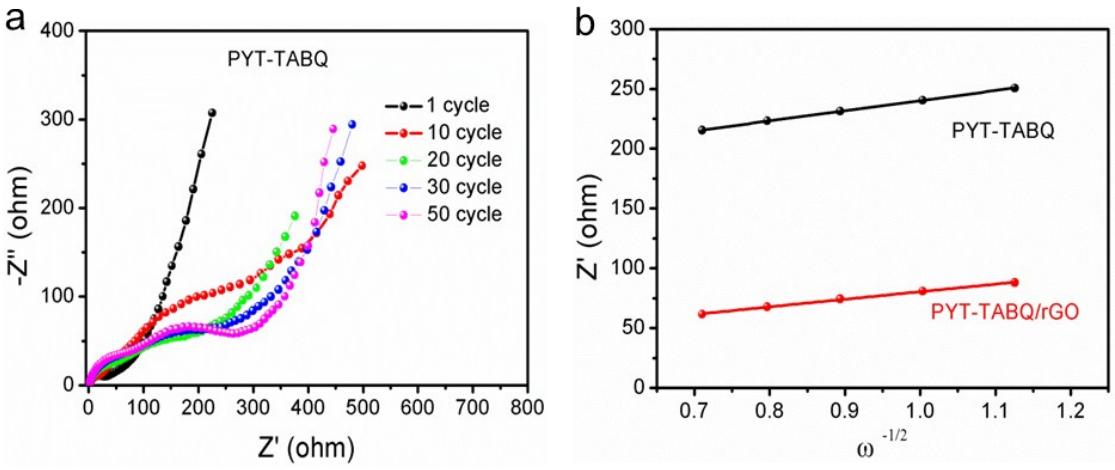

Fig. S16 a) Nyquist plots of the PYT-TABQ and b) The relationship of Z' and $\omega^{-1/2}$ in the low frequency region of PYT-TABQ and PYT-TABQ/rGO, respectively. The increase of the diameter of the semi-circles during cycling indicated the possible irreversible reactions on the surface of the PYT-TABQ electrodes. On the other hand, the charge transfer resistance of the PYT-TABQ/rGO composite electrodes decreased

during cycling, indicating that the PYT-TABQ was protected by the wrapping of rGO in the composite electrodes and the activation process contributed to the charge transfer.

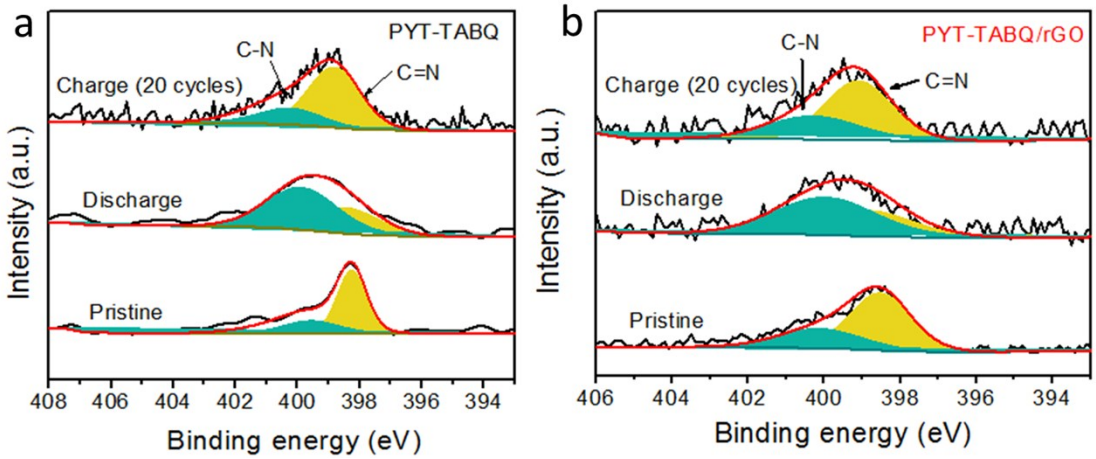

Fig. S17 Ex situ XPS spectra of N 1s of a) PYT-TABQ electrodes and b) PYT-TABQ/rGO composite electrodes during cycling. From the N 1s spectra, during the discharge process, the intensity of C=N bonds (398.4 eV) decreased, accompanying with the strengthening intensity of C-N bonds (399.8 eV). Once being recharged to 3.5 V, the intensity of C-N decreased and the intensity of C=N bonds increased. These results were also observed in the N 1s spectra of the PYT-TABQ/rGO composites in charged and discharged state, which indicated a transformation between the C=N bonds and the C-N bonds during the process of sodiation/desodiation.

The relative intensity of N 1s spectrum of the recharged samples did not completely return to its original state. Furthermore, when the electrodes were cycled after 20

cycles, the PYT-TABQ electrodes also showed lower intensity with obvious noises. These results indicated that the surface of PYT-TABQ electrodes may be covered by the products of the irreversible reactions. On the other hand, the XPS spectra of PYT-TABQ/rGO composite electrodes after recharging are more close to the pristine samples (both of them showed low intensity with noises), indicating that the PYT-TABQ was protected by the wrapping of rGO in the composite electrodes.

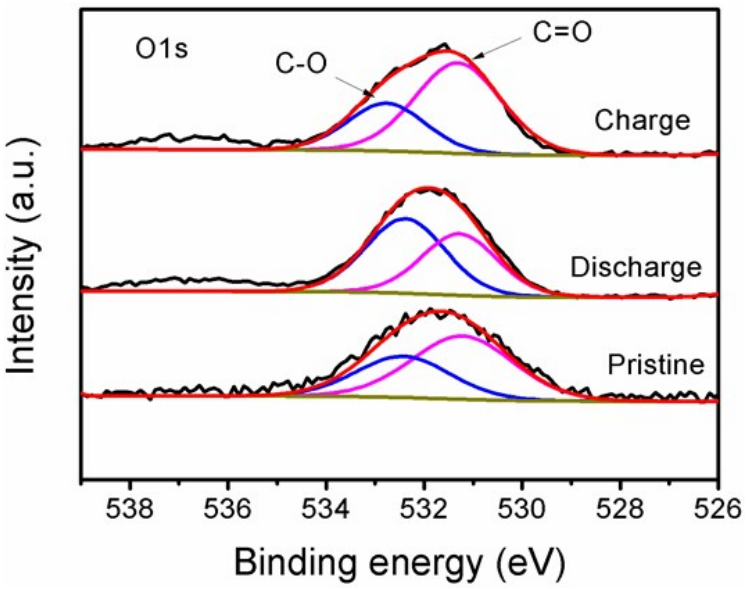

Fig. S18 Ex situ XPS spectra of O 1s during cycling.

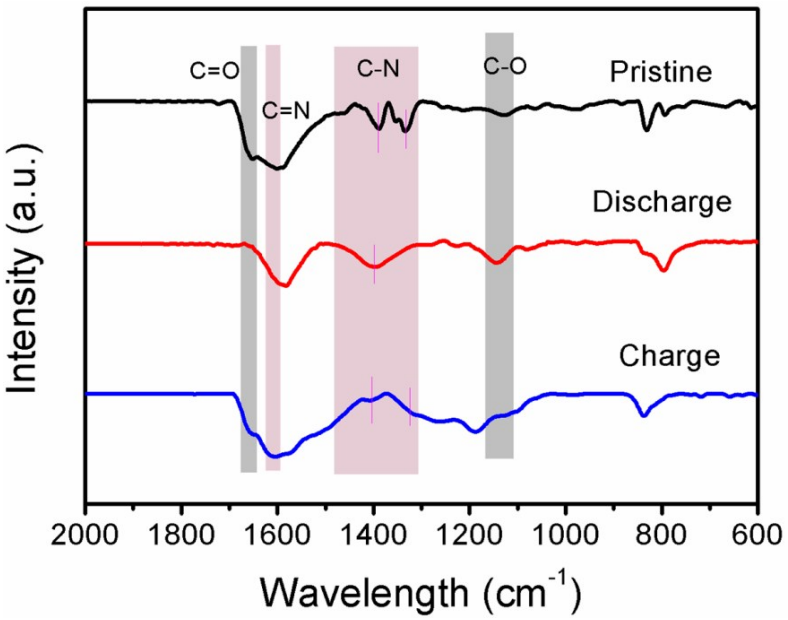

Fig. S19 Ex-FTIR spectra of PYT-TABQ electrodes during cycling.

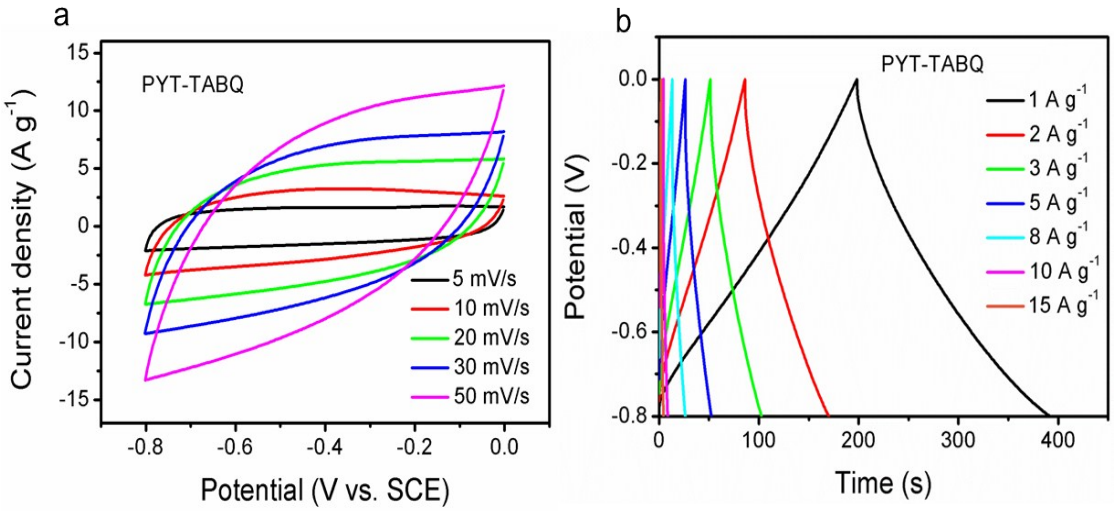

Fig. S20 Electrochemical performance of PYT-TABQ. a) CV curves at different scan rates and b) GCD curves at different current densities.

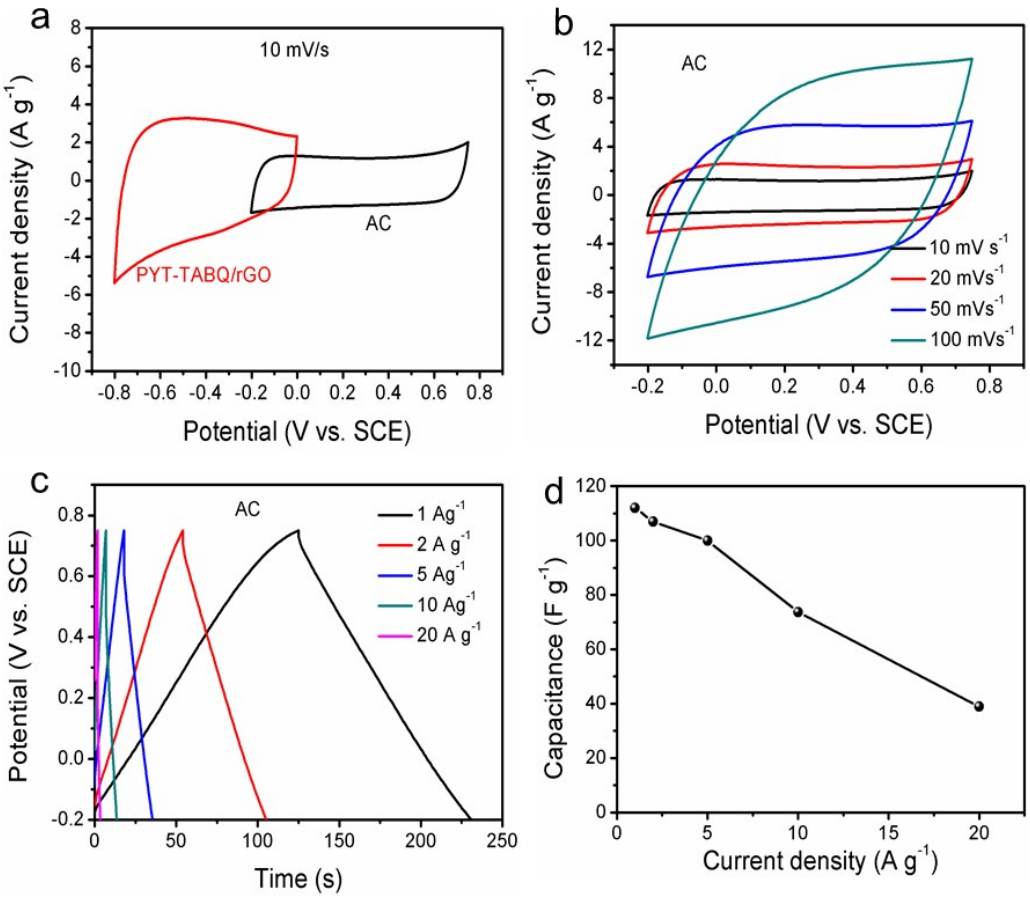

Fig. S21 a) CV curves of the AC and PYT-TABQ/rGO electrodes collected at 10 mV s^{-1}. b) the CV curves, c) GCD curves and d) corresponding capacitance of AC at different scan rates. The nearly rectangular CV curves and linear GCD curves exhibit the typical EDLC characteristics of AC. The specific capacitances of AC calculated by the GCD curves are about 112 F g^{-1} at 1 A g^{-1} and 40 F g^{-1} at 20 A g^{-1} with a retention of about 36%.

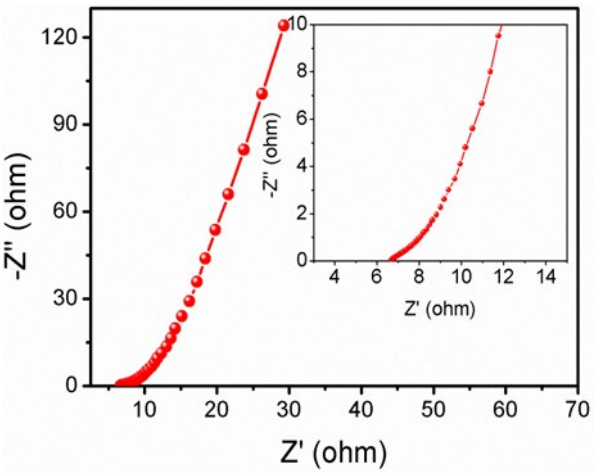

Fig. S22 Nyquist plot of the HSCs with the inset showing high-frequency region. The charge-transfer resistance of the HSCs can be obtained from the size of the semicircle, which is less than 1 Ω.

References

[1] K. Sakaushi, E. Hosono, G. Nickerl, T. Gemming, H. Zhou, S. Kaskel, J. Eckert, Nat. Commun. **2013**, 4, 1485.

[2] W. Deng, X. Liang, X. Wu, J. Qian, Y. Cao, X. Ai, J. Feng, H. Yang, Sci. Rep. **2013**, 3, 2671.

[3] M. Zhou, W. Li, T. Gu, K. Wang, S. Cheng, K. Jiang, Chem. Commun. **2015**, 51, 14354.

[4] L. Zhu, Y. Shen, M. Sun, J. Qian, Y. Cao, X. Ai, H. Yang, Chem. Commun. **2013**, 49, 11370.

[5] H. Li, M. Tang, Y. Wu, Y. Chen, S. Zhu, B. Wang, C. Jiang, E. Wang, C. Wang, J. Phys. Chem. Lett. **2018**, 9, 3205.

[6] Z. Song, Y. Qian, T. Zhang, M. Otani, H. Zhou, Adv. Sci. **2015**, 2, 1500124.

[7] R. Zhao, L. Zhu, Y. Cao, X. Ai, H. X. Yang, Electrochem. Commun. **2012**, 21, 36.

[8] N. Zindy, J. T. Blaskovits, C. Beaumont, J. Michaud-Valcourt, H. Saneifar, P. A. Johnson, D. Bélanger, M. Leclerc, Chem. Mater. **2018**, 30, 6821.

[9] H. Banda, D. Damien, K. Nagarajan, M. Hariharan, M. M. Shaijumon, J. Mater. Chem. A **2015**, 3, 10453.

[10] F. Xu, H. Wang, J. Lin, X. Luo, S.-a. Cao, H. Yang, J. Mater. Chem. A **2016**, 4, 11491.

[11] Y. Zhang, Y. Huang, G. Yang, F. Bu, K. Li, I. Shakir, Y. Xu, ACS Appl. Mater. Interfaces **2017**, 9, 15549.

[12] Y. Huang, K. Li, J. Liu, X. Zhong, X. Duan, I. Shakir, Y. Xu, J. Mater. Chem. A **2017**, 5, 2710.